Article

Polyethylenimine Grafted on Nano-NiFe2O4@SiO2 for the Removal of CrO42–, Ni2+, and Pb2+ Ions from Aqueous Solutions

Mehdi Khalaj *, Seyed-Mola Khatami, Maryam Zarandi, Eric Tobechukwu Anthony, Axel Klein *

Posted Date: 4 December 2023

doi: 10.20944/preprints202312.0194.v1

Keywords: polyethyleneimine; core-shell NiFe2O4@SiO2; magnetic separation; toxic metals; adsorption

Article

Polyethylenimine Grafted on Nano-$NiFe_2O_4$@SiO_2 for the Removal of CrO_4^{2-}, Ni^{2+}, and Pb^{2+} Ions from Aqueous Solutions

Mehdi Khalaj [1,*], Seyed-Mola Khatami [2], Maryam Zarandi [1], Eric Tobechukwu Anthony [3] and Axel Klein [3,*]

[1] Department of Chemistry, Buinzahra Branch, Islamic Azad University, Buinzahra, Iran. Email: khalaj_mehdi@yahoo.com (M.Kj.); Email: maryam.zarandi88@gmail.com (M.Z.)
[2] Department of Chemical Industry, Technical and Vocational University (TVU), Tehran, Iran. Email: molakhatami@gmail.com (S.M.K.)
[3] University of Cologne, Faculty of Mathematics and Natural Sciences, Department of Chemistry, Institute for Inorganic Chemistry, Greinstrasse 6, 50939 Köln, Germany. Email: eanthon2@smail.uni-koeln.de (E.T.A.); Email: axel.klein@uni-koeln.de (A.K.)
* Correspondence: khalaj_mehdi@yahoo.com (M.K.); axel.klein@uni-koeln.de (A.K.)

Abstract: Polyethyleneimine (PEI) has been reported to have good potential for the adsorption of metal ions. In this work, PEI was covalently bound to $NiFe_2O_4$@SiO_2 nanoparticles to form the new adsorbent $NiFe_2O_4$@SiO_2–PEI. The material allowed magnetic separation and was characterized via powder X-ray diffraction (PXRD), field emission scanning electron microscopy (FE-SEM), energy-dispersive X-ray spectroscopy (EDX), Fourier-transform IR spectroscopy (FT-IR), and thermogravimetry-differential thermal analysis (TGA-DTA). The adsorption of CrO_4^{2-}, Ni^{2+}, and Pb^{2+} ions from aqueous solutions was studied at different pH, temperatures, metal ion concentration, and adsorbent dosage. Maximum adsorption capacities of 149.23, 156.68, and 161.25 mg/g were obtained for CrO_4^{2-}, Ni^{2+}, and Pb^{2+}, respectively under optimum conditions using 0.075 g of the adsorbent material 250 mg/L ion concentration, at pH = 6.5 and room temperature.

Keywords polyethyleneimine; core-shell $NiFe_2O_4$@SiO_2; magnetic separation; toxic metals; adsorption

1. Introduction

Toxic metals such as lead have been used by human mankind for thousands of years, but only with the industrial revolution and the rapid growth of the human population and industrial activities in the last 70 years, the penetration of toxic metals into the natural environment and water resources has enormously increased and represents a thread to human health [1]. Many of the metals under concern are heavy metals such as Hg, Cd, and Pb. This is why the term "heavy metals" is frequently used for all toxic metals. However, toxic metals such as Be, Cr, and Ni should not be termed heavy metals as their density does not exceed 5 g/cm^2 and their chemistry is also dissimilar to heavy metals that have a high binding affinity to sulfur-based (bio)ligands in common [1,2].

The detection of toxic metals and their removal from water resources has been continuously an important scientific topic and various methods have been developed to remove toxic metals such as chemical precipitation (including coagulation and flocculation), adsorption, electrochemical reduction, removal through membrane processes, reverse osmosis, and ion exchange methods [3]. Important goals are reducing the costs, simplifying the methods, avoid double contamination, and increase sensitivity [4–7]. Amongst these methods, adsorption (chemi- and physisorption) is the most interesting in terms of sensitivity and selectivity and functionalized nanoparticular materials seem to be favorable for their large surface to mass ratio [4,6,8–14].

Preprints (www.preprints.org) | NOT PEER-REVIEWED | Posted: 4 December 2023 doi:10.20944/preprints202312.0194.v1

From the chemical viewpoint main challenges in the removal of toxic metal ions from wastewater lies in the efficiency and in the recyclability of the adsorbents [3]. Polyethyleneimine (PEI) has been reported to be an efficient material showing fast uptake and fast release under different pH conditions [15–19]. For recovery, most adsorbents were separated and then recycled through centrifugation or filtration but in recent years the use of magnetically separable adsorbent materials was introduced and seems very promising to achieve high recycling rates [5,17,20–23]. Frequently, the magnetic separation is based on hematite and magnetite embedded in core-shell nanoparticles [17,20,24–29] and in recent years hematite and magnetite structures have been successfully replaced with ferrite structures such as nickel ferrite ($NiFe_2O_4$) [30,31], $CoFe_2O_4$ [25,32], or $MnFe_2O_4$ [21,33].

Herein we report a study on the use of polyethylene imine (PEI) grafted on core-shell $NiFe_2O_4@SiO_2$ nanoparticles as adsorbent for the removal of CrO_4^{2-}, Ni^{2+}, and Pb^{2+} ions from water. We studied the influence of parameters such as pH, temperature, metal ion concentration, and amount of $NiFe_2O_4@SiO_2$–PEI adsorbent and also investigated the kinetics of the adsorption system.

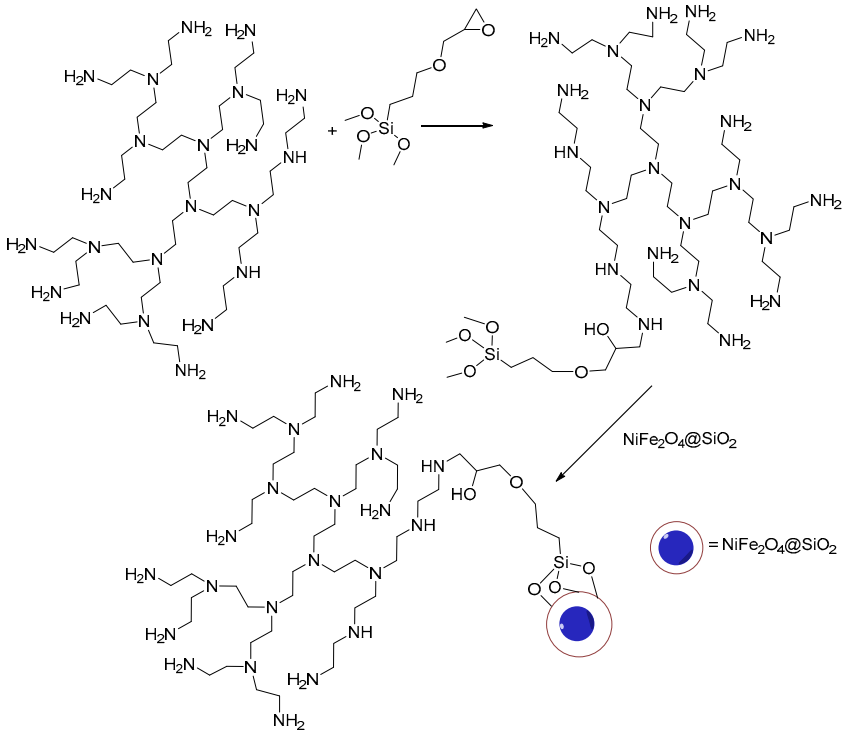

Scheme 1. Preparation of the polyethylene imine (PEI) grafted on core-shell $NiFe_2O_4@SiO_2$ nanoparticles ($NiFe_2O_4@SiO_2$–PEI) though trimethoxy(3-(oxiran-2-yl-methoxy)propyl)silane.

In a recent very similar approach $Fe_3O_4@SiO_2$–PEI–NTDA nanoparticles (NP) in which $Fe_3O_4@SiO_2$ nanoparticles were functionalized with PEI and 1,4,5,8-naphthalenetetracarboxylic-dianhydride (NTDA) were used to adsorb Pb^{2+} ions in the presence of Cd^{2+}, Ni^{2+}, Cu^{2+}, and Zn^{2+} [17]. Further similar materials were Fe_3O_4@MIL-88A(Fe)–APTMS NP based on the Fe-containing MOF MIL-88A(Fe) and (3-aminopropyl)trimethoxysilan (APTMS) applied for the removal of CrO_4^{2-}, Cd^{2+}, and Pb^{2+} [34], $CoFe_2O_4$@MWCNT–CTS NP based on multi-walled carbon nanotubes and chitosan (CTS) for the adsorption of Pb^{2+} [32], $MnFe_2O_4$@GO–TPA based on graphene oxide (GO) and tetraethylenepentamine (TPA) for the adsorption of Pb^{2+} [33], and very recently $Fe_3O_4@SiO_2$–CTS–DTPA with diethylenetriaminepentaacetate (DTPA) binding at the NH functions of CTS for the removal of Pb^{2+} [35]. A similar comparative study for CrO_4^{2-}, Ni^{2+}, and Pb^{2+} (along with Cd^{2+} and Hg^{2+}) was previously led using amino-functionalized Fe_3O_4@GS nanomaterials based on non-further defined graphene (GS) [36]. CrO_4^{2-} was efficiently removed using sodium lignosulfonate/PEI/sodium alginate beads very recently [37]. Very recently polyaniline-grafted pine sawdust was used to efficiently adsorb Cu^{2+}, Co^{2+}, Cd^{2+}, Ni^{2+}, Pb^{2+}, Zn^{2+} and Fe^{2+} in a comparative study [38]. In a very recent

Preprints (www.preprints.org) | NOT PEER-REVIEWED | Posted: 4 December 2023 doi:10.20944/preprints202312.0194.v1

approach, 8-chloroacetyl–aminoquinoline (CAAQ) was attached through PEI as ligand to Fe_3O_4@SiO_2 nanoparticles for the capture of Fe^{3+}, Cu^{2+}, and Cr^{3+} [23].

2. Materials and Methods

2.1. Instrumentation

Powder X-ray diffraction (PXRD) measurements were carried out on a Shimadzu 6100 using Cu-Kα irradiation on solid powder samples of freshly prepared and recovered materials of $NiFe_2O_4$@SiO_2-PEI. PXRD of $NiFe_2O_4$ were recorded on an STOE-STADI MP diffractometer equipped with a Cu-Kα_1 radiation (λ = 0.15406 Å) source and operating in transmission mode. Atomic absorption spectroscopy (AAS) was measured using a Shimadzu AA-6880 spectrophotometer. TGA-DTA was recorded on a Shimadzu TGA-DTG-60H instrument. FT-IR spectra were recorded on a Bruker Alpha I spectrophotometer on KBr disks. FE-SEM and EDX analysis were carried out on a JEOL JSM-IT 100 instrument.

2.2. Reagents

All chemicals including $NiCl_2{\cdot}6H_2O$, $FeCl_3{\cdot}6H_2O$, $FeCl_2{\cdot}6H_2O$, $Si(OEt)_4$, trimethoxy(3-(oxiran-2-ylmethoxy)propyl)silane, and toluene were purchased from Merck and Sigma-Aldrich and used without further purification.

2.3. Synthesis of the $NiFe_2O_4$@SiO_2–PEI adsorbent

$NiFe_2O_4$@SiO_2 was prepared according to our previously reported work [30]. In brief, 10 g of PEI (Sigma-Aldrich, 5000 average molecular weight) were dissolved in 50 mL hot toluene and then cooled. This was mixed with 472 mg (2 mmol) trimethoxy(3-(oxiran-2-yl-methoxy)propyl)silane (M_W = 248.35 g/mol, from Sigma-Aldrich) and the mixture heated under reflux for 8 h. Then, 2.5 g of the $NiFe_2O_4$@SiO_2 nanoparticles were added at room temperature and the mixture was heated under reflux for 5 h. The resulting colorless solid was filtered, washed with toluene, and dried at 50 °C. For the analytics, see the results and discussion section.

2.4. Adsorption experiments

For the metal standard solutions 5, 10, 15, 20, 25, and 30 mg/L of $Na_2Cr_2O_7{\cdot}2H_2O$ (for CrO_4^{2-}, M_W = 297.99 g/mol), $Ni(NO_3)_2{\cdot}6H_2O$ (for Ni^{2+}, M_W = 229.54 g/mol), and $Pb(NO_3)_2.6H_2O$ (for Pb^{2+}, M_W = 370.84 g/mol) were dissolved in 100 mL deionized water. This translates to 0.3356–2.0135 mmol/L for CrO_4^{2-}, Ni^{2+}, and Pb^{2+}, 0.2178–1.3070 mmol/L for Ni^{2+}, and 0.1348–0.8090 mmol/L for Pb^{2+}. The pH was adjusted to 3 to 8 using diluted NaOH (1M) or HCl (1M) solutions. Adsorption procedure: A 250 mL Erlenmeyer flask was equipped with 50 mL of each metal ion solution (50–300 mg/L), the adsorbent (0.01–0.1 g) was added and the mixture was stirred at room temperature for 45 min at pH values ranging from 3 to 8.

The adsorption capacity at equilibrium (q_e) and the adsorption capacity at time t (q_t) are defined as:

$$q_e = \frac{(C_0\text{-}C_e)V}{m} \qquad q_t = \frac{(C_0\text{-}C_t)V}{m}$$

with C_0: initial concentration (mg/L), C_e: equilibrium concentration(mg/L), m: amount of adsorbent (g), V: volume of the solution (L) [39].

2.5. Adsorbent recovery

After adsorption of the CrO_4^{2-}, Ni^{2+}, and Pb^{2+} ions at pH = 6.5; 0.075 g adsorbent; 250 mg/L metal ions; 298 K for 45 min, the magnetic adsorbent was separated from the reaction batch with the help

Preprints (www.preprints.org) | NOT PEER-REVIEWED | Posted: 4 December 2023 doi:10.20944/preprints202312.0194.v1

of an external magnet and was recycled by washing with HCl solution (5%) followed by NaOH solution (5%) to remove the metals.

3. Results and discussion

3.1. Synthesis and characterization of the adsorbent

The $NiFe_2O_4$@SiO_2–PEI adsorbent was prepared as shown in Scheme 1. First, trimethoxy(3-(oxiran-2-ylmethoxy)propyl)silane was reacted with the PEI polymer followed by reaction with core-shell $NiFe_2O_4$@SiO_2 nanoparticles (details in the Materials and Methods Section).

The powder XRD pattern of the $NiFe_2O_4$@SiO_2–PEI adsorbent showed signals at 2Θ = 37.3, 43.4, 46.8, 53.7, 57.7, 62.9, 71.4, and 74.6 ° characteristic for the cubic phase of magnetite and nickel ferrite ($NiFe_2O_4$, reference code: 00-003-0875) while reflections corresponding to silica were absent (Figure 1).

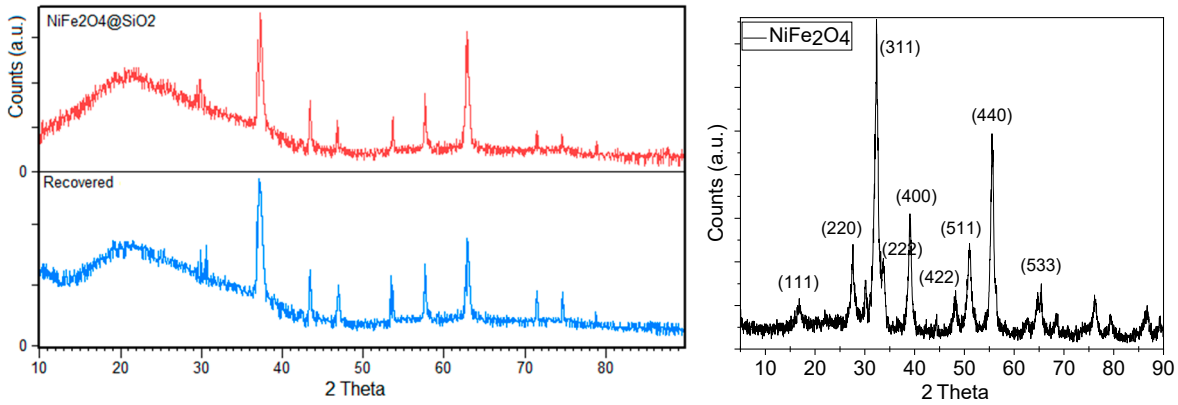

Figure 1. XRD pattern of $NiFe_2O_4$@SiO_2–PEI (left) and of pristine $NiFe_2O_4$ (right).

The FT-IR analysis of $NiFe_2O_4$@SiO_2–PEI (Figure 2) showed bands at 3678, 3609, and 3573 cm^{-1} assignable to N–H stretching vibrations, the broad peak between 3100 and 3700 cm^{-1} is due to O–H stretching modes, while C(sp^3)–H stretches appear sharp at 2945 and 2879 cm^{-1}. The C–H bending modes are found at 1348 cm^{-1}. The bands located at 1634, 1210, 1153, 1110, 1038, 924, and 879, cm^{-1} can be assigned to the Si–O–Si, Si–O, C–C, C–N, and C–O functionalities. Finally, the Fe–O lattice vibrations appear as a broad band centered at 530 cm^{-1} [23,30,37].

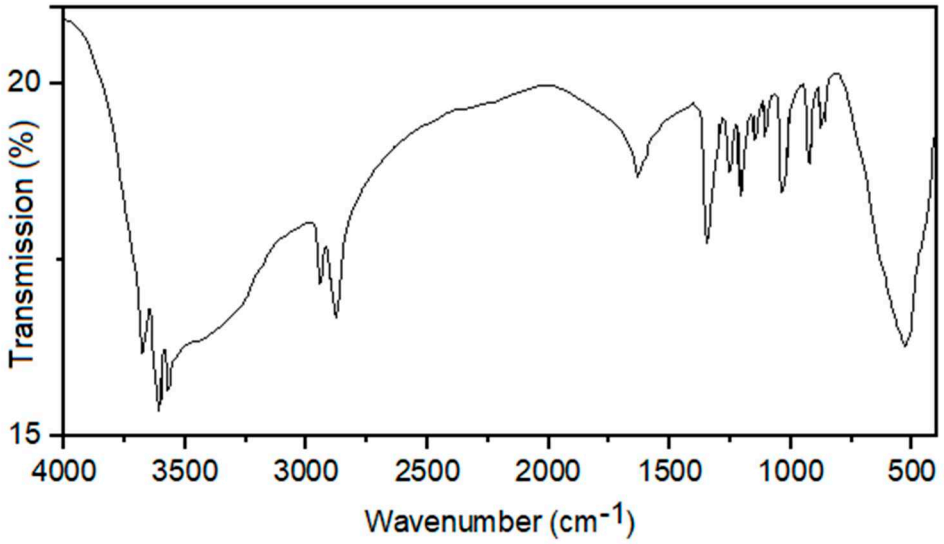

Figure 2. FT-IR spectrum of $NiFe_2O_4$@SiO_2–PEI.

Preprints (www.preprints.org) | NOT PEER-REVIEWED | Posted: 4 December 2023 doi:10.20944/preprints202312.0194.v1

Field emission scanning electron microscopy (FE-SEM) images of $NiFe_2O_4$@SiO_2–PEI show irregular shaped and partially agglomerated particles with diameters ranging from 50 to 100 nm (Figure 3) similar to what we recently reported for $NiFe_2O_4$@SiO_2–PSA particles (PSA = propylsulfonic acid) that were prepared in a similar manner [30]. Energy-dispersive X-ray spectroscopy (EDX) analysis showed C (36.31%), N (38.96%), Ni (2.12%), O (6.78%), Fe (4.38%), and Si (4.12%) (Figure 3).

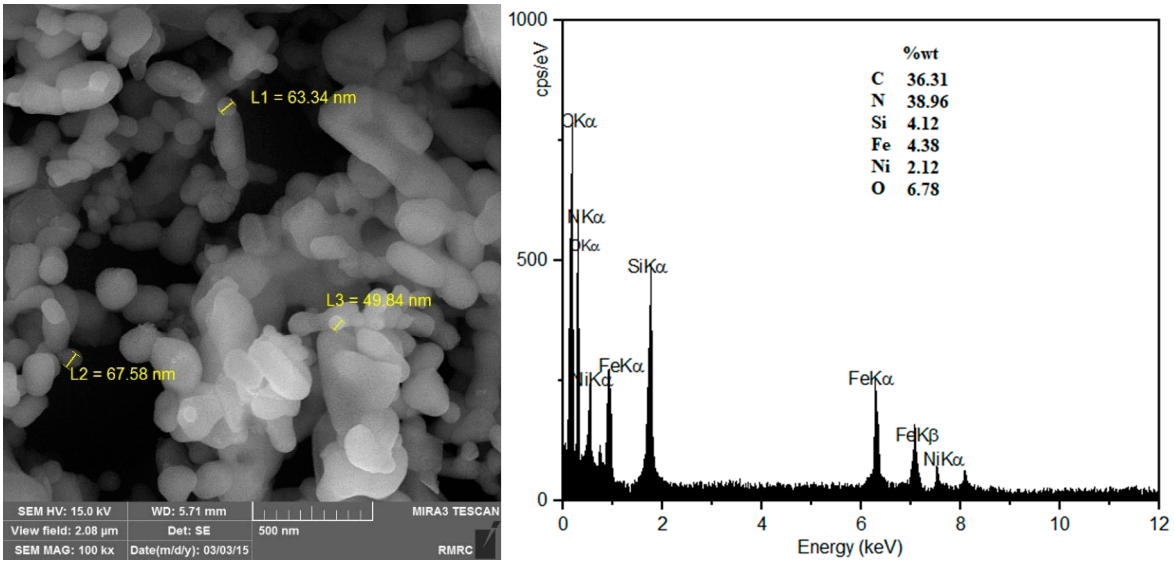

Figure 3. FE-SEM photograph (left) and EDX analysis (right) of $NiFe_2O_4$@SiO_2–PEI.

Thermogravimetric (TGA) and differential thermal analysis (DTA) showed a small weight loss of about 5% around 100 °C which is due to loss of adsorbed water. The major weight of about 77% of the original mass occurred in the range 200 to 500 °C (Figure 4). The residual 18% represent the $NiFe_2O_4$@SiO_2 nanoparticles without the "organic" functionalization in excellent agreement with the EDX analysis showing a total of 75% for C and N.

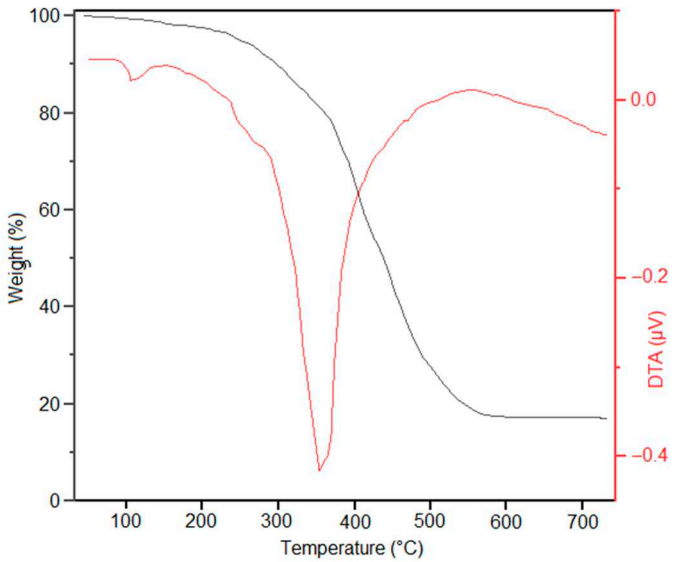

Figure 4. TGA and DTA analysis of $NiFe_2O_4$@SiO_2–PEI.

Preprints (www.preprints.org) | NOT PEER-REVIEWED | Posted: 4 December 2023 doi:10.20944/preprints202312.0194.v1

3.2. Adsorption studies for CrO_4^{2-}, Ni^{2+}, and Pb^{2+} ions

3.2.1. Effect of the pH

In order to evaluate the effect of pH on the adsorption of CrO_4^{2-}, Ni^{2+}, and Pb^{2+}, the pH war varied from 3 to 8 was while other parameters are fixed at 250 mg/L metal ion initial concentration, 0.075g adsorbent, 50 mL volume, and 298 K. The adsorption capacity showed a maximum at a pH of 6.5 and decreased with increasing pH (Figure 5). In acidic media at pH < 6 we assume a competition between protons (H^+) and the metal ions Ni^{2+} and Pb^{2+} in their coordination to the NH_2 groups of the adsorbent. The maximum is reached at pH = 6.5 with adsorption capacities of 149.25, 156.68, and 161.25 mg/g for CrO_4^{2-}, Ni^{2+}, and Pb^{2+}, respectively.

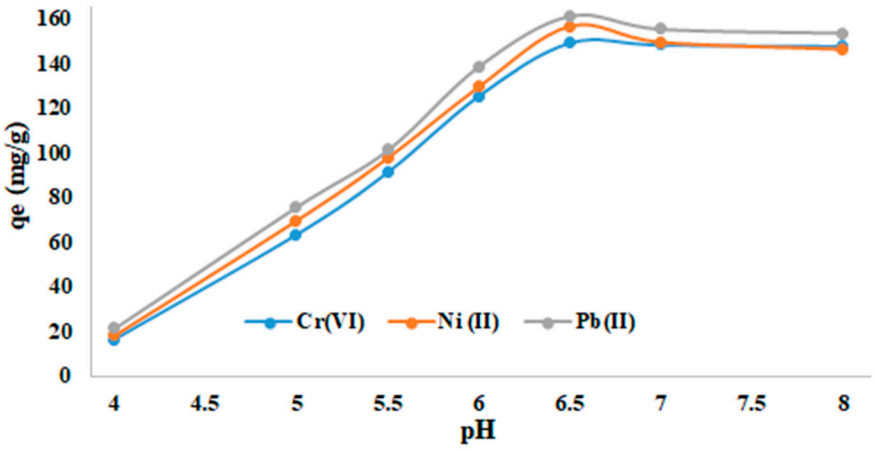

Figure 5. Adsorption of CrO_4^{2-}, Ni^{2+}, and Pb^{2+} ions: effect of the pH (45 min; 0.075 g adsorbent; 250 mg/L adsorbate, 298 K).

Very similar pH-dependent behavior as our materials with the maximum adsorption at pH = 6 was previously reported for the Pb^{2+}-adsorbing materials Fe_3O_4@SiO_2@PEI–NTDA [17], PEI-bacterial cellulose [19], and sodium alginate (ALG)/PEI composite hydrogels [16], in line with PEI acting as coordinating agent in these materials. However, also for Fe_3O_4@SiO_2@PEI–CAAQ in which CAAQ acts as additional ligand [23] the same behavior was found. The very recently reported adsorbent Fe_3O_4@SiO_2–CTS–DTPA (DTPA = diethylenetriaminepentaacetate) [35] shows a maximum Pb^{2+} adsorption already in acidic solutions at pH = 3 and no loss of binding capacity between pH = 3 and pH = 6.

On the other hand, the very similar behavior of our adsorbent towards the cations Ni^{2+} and Pb^{2+} on one side and the anionic CrO_4^{2-} is peculiar as for other amine-containing materials such as the recently reported sodium lignosulfonate/PEI/sodium alginate beads [37], the ethylenediamine-functionalized Fe_3O_4 (EDA@Fe_3O_4) particles [40], amino-functionalized Fe_3O_4@GS nanomaterials [36], polydopamine modified chitosan aerogels [41], or the MOF APTMS@MIL-88A(Fe) (APTMS = (3-aminopropyl)trimethoxysilan) [34], better CrO_4^{2-} adsorption was found at low pH (2 to 3) while cation adsorption is superior at higher pH. This is reasonable in view of the protonated amine functions at low pH allowing to strongly adsorb the CrO_4^{2-} anion while neutral amine function coordinate cations. The only explanation we have so far is that the CrO_4^{2-} has been largely reduced to Cr^{3+} ions which then would absorb in a similar way as Ni^{2+} and Pb^{2+}. This idea is supported by several reports that could show that Cr^{3+} can be formed from CrO_4^{2-} through electron transfer from various materials [15,18,26,37,41–44]. Such CrO_4^{2-} to Cr^{3+} reduction upon adsorption can be very efficient if a distinct electron-donating material is present as in the CTAB-intercalated MoS_2 nanosheets (CTAB = cetyl trimethyl ammonium bromide) that can be used for the simultaneous removal of Cr(IV) and Ni(II) [45] or in the chitosan-modified multi-walled carbon nanotube composites (MWCNT-CTS) that adsorb CrO_4^{2-} exclusively as Cr^{3+} [46].

In future studies we will use X-ray photoelectron spectroscopy (XPS) to study the oxidations states of the adsorbed Cr as was done in the last two mentioned studies.

Preprints (www.preprints.org) | NOT PEER-REVIEWED | Posted: 4 December 2023 doi:10.20944/preprints202312.0194.v1

3.2.2. Effect of the contact time

Examining the effect of contact time in the adsorption process of the metals allowed us calculating the reaction rate and the time to reach equilibrium. For this purpose, the reaction parameters were kept constant with an initial concentration of metal salts of 250 mg/L, 0.075 g adsorbent, and pH = 6.5. The adsorption capacity increased rapidly within the first 5 min, at high rate within the first 20 min and then continues slowly. An almost equilibrium was reached within 45 min (Figure 6).

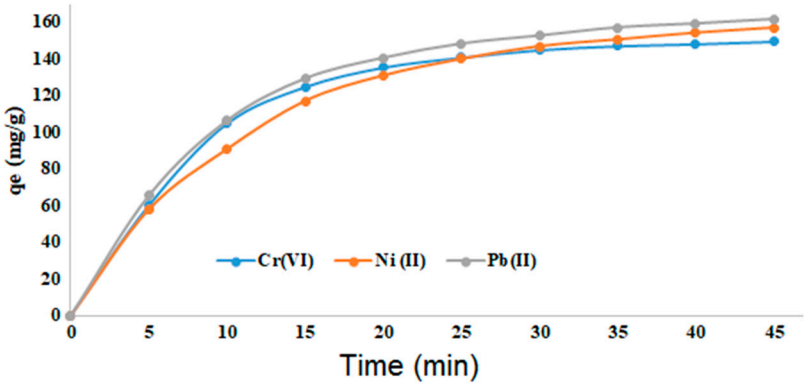

Figure 6. Adsorption of CrO_4^{2-}, Ni^{2+}, and Pb^{2+} ions over time (pH = 6.5; 0.075 g adsorbent; 250 mg/L metal ions; 298 K).

For the previously reported similar materials Fe_3O_4@SiO_2@PEI–NTDA [17] and Fe_3O_4@SiO_2@PEI–CAAQ [23], the adsorption capacities reached plateau values only after more than 200 min [17] or 90 min [23], respectively which indicates that our system is markedly more active and lies in the same time-range as the previously reported PEI-bacterial cellulose [19]. In contrast to this, very fast adsorption of Cu^{2+}, Co^{2+}, Cd^{2+}, Ni^{2+}, Pb^{2+}, Zn^{2+} and Fe^{3+} within 10 to 20 min was achieved with polyaniline grafted on pine saw dust [38], underlining the suitability of polyamines and anilines in efficiently coordinating the metals.

3.3. Adsorption kinetic and mechanism

The mechanism of the adsorption of the metal ions were studied *via* different kinetic models e.g. pseudo-first order, pseudo-second order, and Elovich models [47]. The correlation coefficient (R^2) values for the different kinetic models were calculated by drawing $\log(q_e–q_t)$ *vs.* t (pseudo-first order), t/q_t *vs.* t (pseudo-second order), and q_t *vs* ln t (Elovich) diagrams (Table 1). The agreement with pseudo-first order kinetics is slightly better than the pseudo-second order fit and much better than with the Elovich equation. This stands in contrast to the behavior of the reported adsorption of Pb^{2+} by an activated carbon [47] and we ascribe this to the more unspecific surface of the carbon in contrast to the well-defined coordination sites of PEI. This is supported by the very similar behavior of the Fe_3O_4@SiO_2@PEI–NTDA [17] that showed also pseudo-first order kinetics for the Pb^{2+} adsorption. The better agreement of experimental data with pseudo-second order kinetics reported for Fe_3O_4@SiO_2@PEI–CAAQ [23] is in line with the additional CAAQ ligand showing superior binding than PEI.

Table 1. Parameters and correlation coefficient (R^2) of kinetic models.

Linear equations [a]	**Parameters**								
	CrO_4^{2-}			**Ni^{2+}**			Pb^{2+}		
Pseudo-first order	***k***	***R*²**	**$q_{e\ (mg/g)}$**	***k***	R^2	$q_{e\ (mg/g)}$	k	R^2	$q_{e\ (mg/g)}$
	0.118	0.999	151.07	0.097	0.992	169.78	0.102	0.996	159.66
Pseudo-second order	0.0014	0.981	163.93	0.0008	0.968	175.43	0.0011	0.980	178.57
Elovich equation	α	R^2	β	α	R^2	β	α	R^2	β

Preprints (www.preprints.org) | NOT PEER-REVIEWED | Posted: 4 December 2023 doi:10.20944/preprints202312.0194.v1

	135.57	0.928	0.026	10.85	0.983	0.022	79.89	0.963	0.023

[a] Pseudo-first order: $\log(q_e - q_t) = \log q_e (k\,t\,/2.303)$ with k is the rate constant (min^{-1}), t is the contact time (min),
Pseudo-second order: $t/q_t = (1/kq_e^2)+(t/q_e)$, Elovich equation: $qt = (\ln(\alpha\beta)/\beta)+(\ln t/\beta)$ with β, α are the Elovich constants.

3.3.1. Effect of the amount of adsorbent

The effect of the amount of adsorbent was studied in the range from 0.01 g to 0.1 g while other parameters are held constant (conc. of adsorbates: 250 mg/L, pH = 6.5). With increasing amounts of adsorbent, the adsorption capacity increased up to about 0.08 g (Figure 7). Further increase did not give higher adsorption. The slight decrease in adsorption capacity at high adsorbent loads might be due to aggregation and accumulation of particles and overall reduction of their surface.

A marked maximum adsorption maximum for Pb^{2+} was found in the dosage-behavior for the recently reported adsorbent material Fe_3O_4@SiO_2@PEI-NTDA [17]. For this material also, aggregation was assumed to be responsible for this phenomenon. When comparing the two curves, our maximum is less pronounced, meaning that our system is more tolerant to larger amounts of adsorbent.

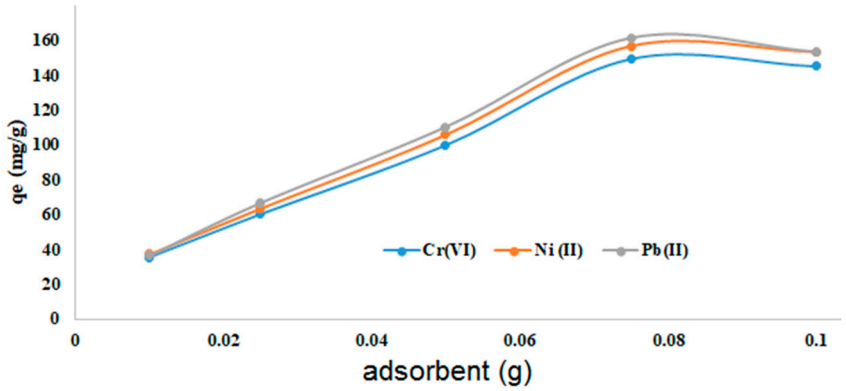

Figure 7. Adsorption of CrO_4^{2-}, Ni^{2+}, and Pb^{2+} ions: effect of adsorbent amount (45 min; pH = 6.5; 250 mg/L adsorbates; 298 K).

3.3.2. Effect of the metal ion concentration

In order to determine the maximum adsorption capacity of the adsorbent, the effect of different concentrations of metal ions was evaluated. Figure 8 shows that the adsorption capacity of the adsorbent increases with the increase of the initial concentration of CrO_4^{2-}, Ni^{2+}, and Pb^{2+} ions. The highest adsorption capacity was observed at a concentration of 250 mg/L. At higher concentrations, the adsorption capacity of the adsorbent remains constant pointing to the saturation of the adsorbent sites.

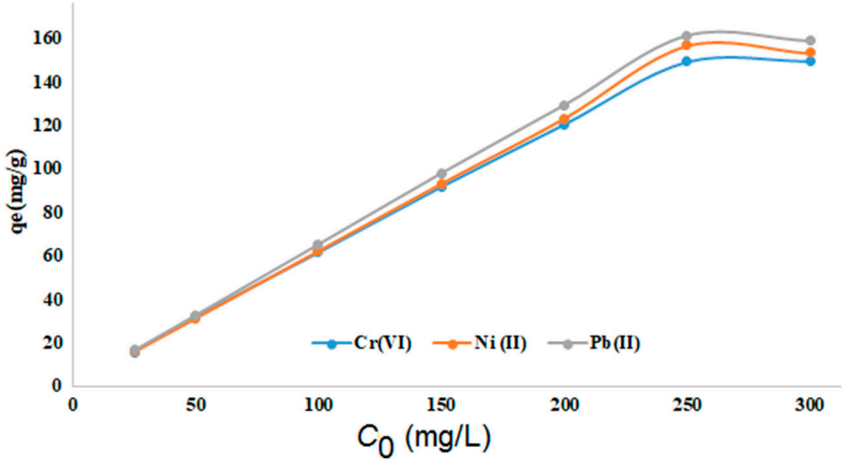

 doi:10.20944/preprints202312.0194.v1

Figure 8. Adsorption of CrO_4^{2-}, Ni^{2+}, and Pb^{2+} ions: effect of initial metal ion concentration (45 min; 0.075 g adsorbent; pH = 6.5; 298 K).

3.4. Adsorption isotherms

The equilibrium isotherm studies could provide the information about the nature of the interaction between the adsorbed material and the adsorbent and can be used to determine the adsorption capacity of the adsorbent. In order to conduct a view of the way of CrO_4^{2-}, Ni^{2+}, and Pb^{2+} ions adsorption, the mechanism was investigated by applying the linear forms of Langmuir, Freundlich, and Temkin isotherm models [48]. The calculated parameters for different isotherms are depicted in Table 2. By looking at the parameters of isotherms we are able to get an insight into the adsorption mechanism. The Langmuir isotherm model is based on the hypothesis that a single-layer of adsorbent material on the surface structure of the adsorbent is saturated during adsorption, the adsorption sites are identical, the energy of the adsorption is not dependent on the surface coverage, and there is no interaction between the adsorbates (here, the adsorbed metal ions) [47].

Table 2. Parameters and correlation coefficient (R^2) of isotherm models.

	CrO_4^{2-}			Ni^{2+}			Pb^{2+}		
Model	**Parameters**								
Langmuir	**b**	R^2	$q_{max\ (mg/g)}$	b	R^2	$q_{max\ (mg/g)}$	b	R^2	$q_{max\ (mg/g)}$
	0.075	0.972	181.81	0.105	0.976	178.57	0.441	0.997	166.67
Freundlich	k_f	R^2	n	k_f	R^2	n	k_f	R^2	n
	0.015	0.910	0.646	0.016	0.893	0.675	0.0014	0.814	0.553
Temkin	B	R^2	A	B	R^2	A	B	R^2	A
	0.0247	0.931	367.1	0.0226	0.885	298.3	0.0272	0.838	1.584

a qmax is the maximum monolayer adsorption capacity (mg/g); qe is the sorption capacity at equilibrium (mg/g); Ce is the concentration of CrO42– at equilibrium (mg/L). R2 is the correlation coefficient.: Langmuir linear equation: Ce/qe = 1/bqmax + Ce/qmax with b (L/mg) is the Langmuir constant; Freundlich linear equation: lnqe = lnkf + lnCe/n with kf and n are the Freundlich constants; Temkin linear equation: qe = BlnA + BlnCe with A and B are the Temkin constants.

The correlation coefficient (R^2) was calculated for all isotherms and fitted to the experimental data. Values of 0.972 (CrO_4^{2-}), 0.976 (Ni^{2+}), and 0.997 (Pb^{2+}) R^2 show that the Langmuir isotherm fitting agrees very well with the experimental results. Accordingly, the mechanism of the adsorption is monolayer adsorption on the surface of the adsorbent [48,49]. The same behavior was also found for similar adsorbent materials such as Fe_3O_4@SiO_2@PEI–CAAQ [23], Fe_3O_4@SiO_2@PEI–NTDA [17], and Fe_3O_4@SiO_2–CTS/DTPA [35], while for the CrO_4^{2-} adsorption on sodium lignosulfonate/PEI/sodium alginate beads [37] the Langmuir and Freundlich models gave very similar R^2 values. The Freundlich isotherm applies to non-ideal adsorption on heterogeneous surfaces [50,51] and the Freundlich-type of behavior is in line with the very heterogeneous surface of the lignosulfonate/PEI/sodium alginate material [37] in contrast to our adsorbent.

3.5. Adsorption thermodynamics

The effect of temperature on the adsorption capacity was investigated to determine the thermodynamic parameters and investigate the spontaneity of the adsorption process. The adsorption capacity decreased with increasing temperature from room temperature to 75°C (Figure 9). This is in line with an exothermic nature of the adsorption process.

Preprints (www.preprints.org) | NOT PEER-REVIEWED | Posted: 4 December 2023 doi:10.20944/preprints202312.0194.v1

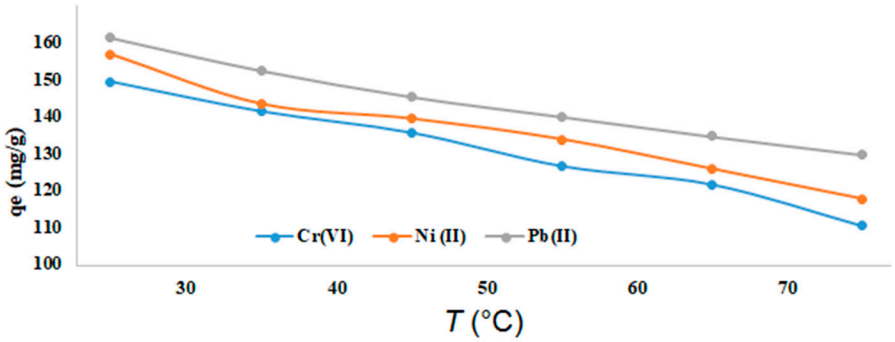

Figure 9. Adsorption of CrO_4^{2-}, Ni^{2+}, and Pb^{2+} ions over *T* (45 min; 0.075 g adsorbent; 250 mg/L metal ion conc. concentration; pH = 6.5).

From this data, we calculated also the Gibbs free energy (ΔG), enthalpy (ΔH), and entropy (ΔS) of the system. The change in ΔG of the CrO_4^{2-}, Ni^{2+}, and Pb^{2+} ions at six different temperatures is obtained through the relationships between ΔG, ΔH, ΔS and ln Kc in the equations shown in Table 3. ΔH and ΔS are obtained by plotting ln Kc against 1/*T* (Figure 10).

Thermodynamic parameters ΔG, ΔH and ΔS are shown in Table 3. The negative value of ΔG is in line with spontaneous adsorption processes on the surface of the adsorbent. The negative values of ΔH and ΔS show the exothermic nature of the adsorption reaction, which is very probably binding to the amine functions of the PEI. The overall exothermic binding is in line with the rapid binding (compare Figure 6) and is an important pre-requisite for the use of this material for efficient metal-recovery from solution.

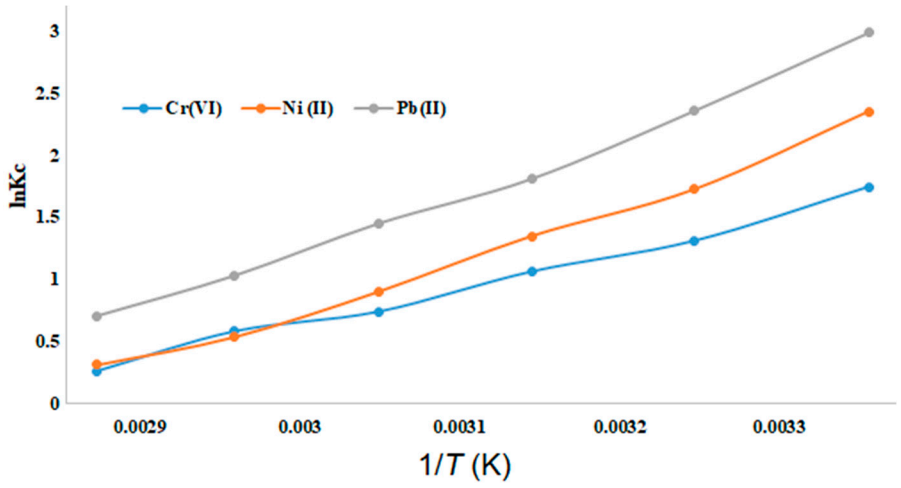

Figure 10. Linear plot of ln K_c *vs* 1/*T* for the adsorption of CrO_4^{2-}, Ni^{2+}, and Pb^{2+} ions.

Table 3. Thermodynamic parameters for the adsorption of CrO_4^{2-}, Ni^{2+}, and Pb^{2+} ions.[a]

ΔG° (kJ/mol) (*T* = 298 K)			**ΔS° (J/K·mol)**			ΔH° (kJ/mol)		
CrO_4^{2-}	**Ni^{2+}**	**Pb^{2+}**	**CrO_4^{2-}**	**Ni^{2+}**	**Pb^{2+}**	CrO_4^{2-}	Ni^{2+}	Pb^{2+}
–4.18	–5.58	–7.37	–67.96	–98.92	–106.64	–24.43	–35.06	–38.96

[a] Kc (L/mg) is the equilibrium constant, R = 8.314 J/mol·K, *T* is the absolute temperature (K), Gibbs free energy ΔG°(kJ/mol), Enthalpy ΔH°(kJ/mol), Entropy ΔS° (J/K·mol). $\Delta G^0 = -RT\ln K_C$ with $K_C = q_e/C_e$ and $RT\ln K_C = T\Delta S^0 \cdot \Delta H^0$.

As in the pH-dependent experiments, the anionic CrO_4^{2-} behaves remarkably similar to the Ni^{2+} and Pb^{2+} cations with negative ΔH^0, ΔS^0, and ΔG^0. This stands in contrast to the related sodium lignosulfonate/PEI/sodium alginate beads for which the CrO_4^{2-} adsorption showed positive ΔH^0 (7.5 kJ/mol) and ΔS^0 (70 J/K·mol) values, but a negative ΔG^0 of –13.36 kJmol^{-1} at 298 K [37]. This difference

 doi:10.20944/preprints202312.0194.v1

supports our assumption that the CrO_4^{2-} ions in our test solutions are adsorbed as Cr^{3+} ions on the adsorbent.

3.6. Scanning electron microscope (SEM) / energy-dispersive X-ray (EDX) analysis

Figure 11A shows the SEM image of the as-prepared $NiFe_2O_4$@SiO_2-PEI adsorbent having a cauliflower-like morphology. The morphology does not change upon loading with Cr(VI), Pb(II) and Ni(II) (Figure 11B to 11D). EDX spectra show the characteristic peaks of Cr(VI), Pb(II) and Ni(II) ions (Figure 11F to 11G). For comparison we recorded the EDX of a re-cycled $NiFe_2O_4$@$SiO_{2\#}$-PEI sample and we found traces of Na^+ and Cl^- (Figure 11E) stemming from the washing procedure (first HCl, then NaOH, see Materials and Methods).

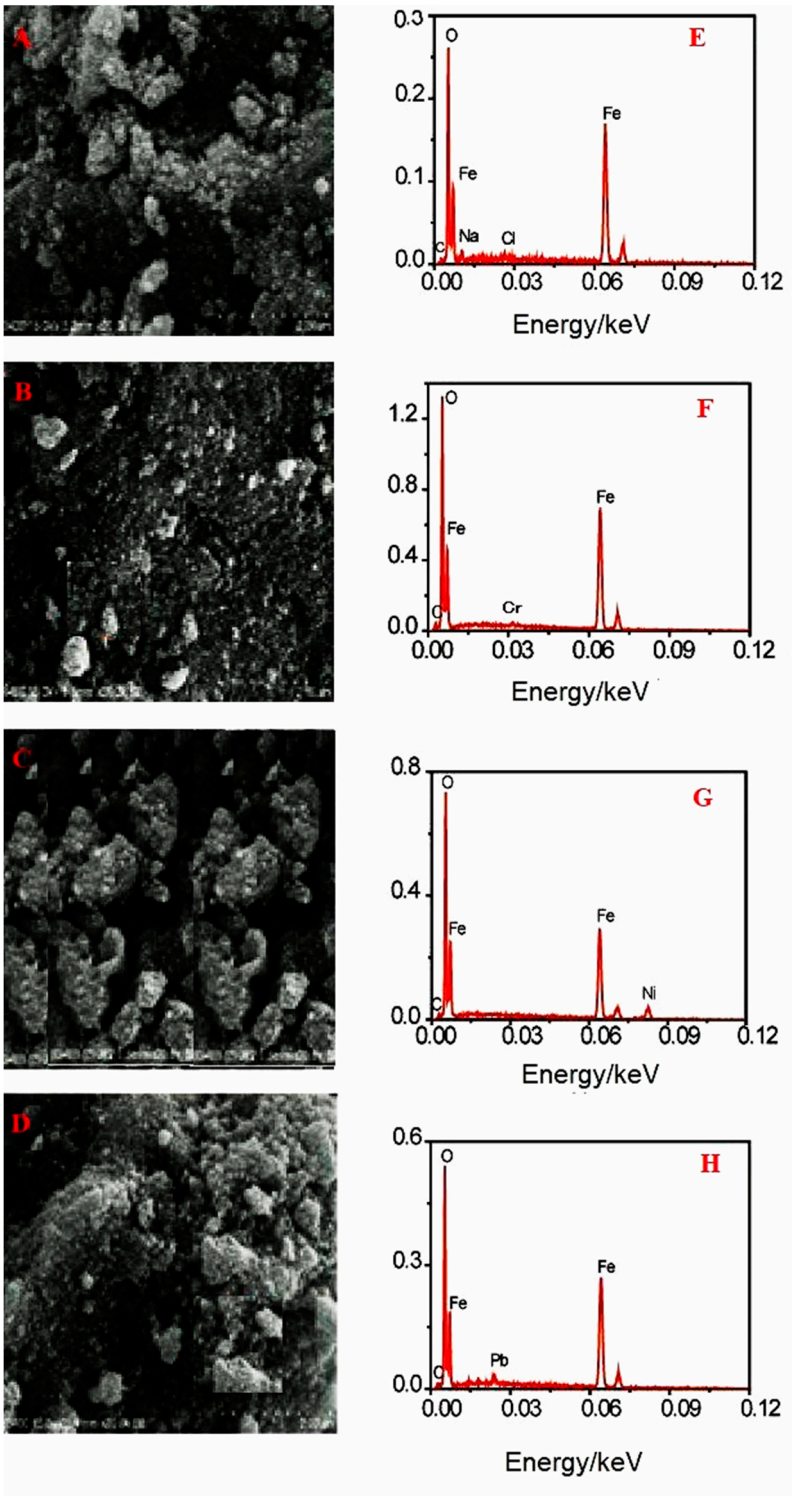

Preprints (www.preprints.org) | NOT PEER-REVIEWED | Posted: 4 December 2023 doi:10.20944/preprints202312.0194.v1

Figure 11. SEM images of $NiFe_2O_4@SiO_2$–PEI before (A) and after Cr(VI) (B), Ni(II) (C), and Pb(II) (D) adsorption. EDX spectra of recovered $NiFe_2O_4@SiO_2$–PEI before metal ion adsorption (E) and after Cr(VI) (F), Ni(II) (G), and Pb(II) (H) adsorption. (Metal concentrations 10 mg L^{-1}). Scale bars in A to D: S3400 15.0 kV 5.2 mm x 20.0 k SE (2.00 μm).

3.7. Adsorbent recovery

The recyclability was tested in 11 consecutive runs and the adsorbent showed good recovery (Figure 12) for all three ions.

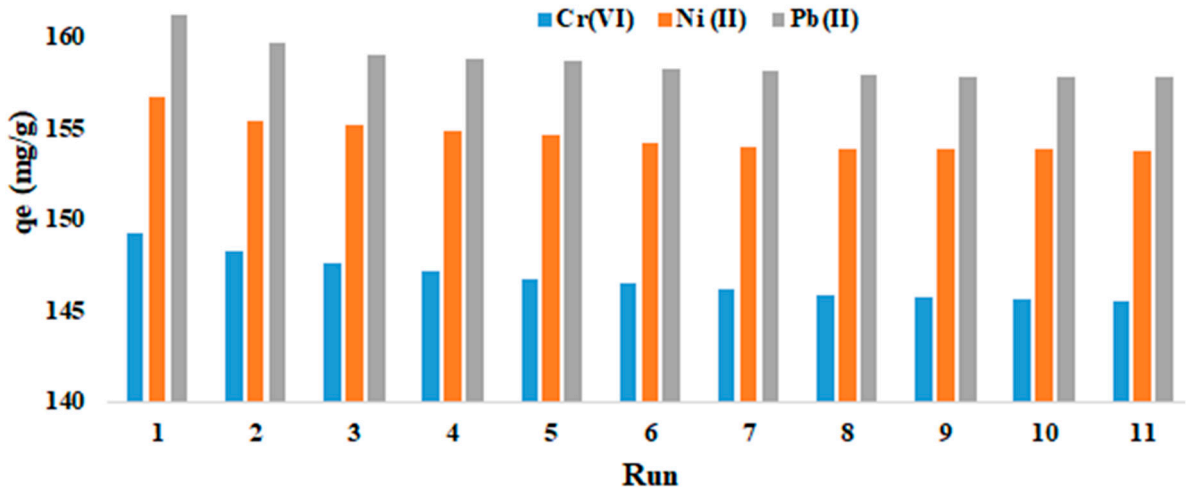

Figure 12. Adsorption of CrO_4^{2-}, Ni^{2+}, and Pb^{2+} ions at pH = 6.5; 0.075 g adsorbent; 250 mg/L metal ions; 298 K for 45 min in 11 consecutive runs.

For the recently reported $Fe_3O_4@SiO_2$@PEI–CAAQ (CAAQ = 8-chloroacetyl–aminoquinoline) [23], efficient recycling was only achieved when using Na_2EDTA^{2+} solutions for the stripping of the metal cations, while desorption using HCl or HNO_3 steadily decreased the adsorption capacity. This underlines that the additional CAAQ ligand helps to stronger bind metal cations, but at the same time is detrimental to a rapid and efficient desorption.

4. Conclusions

In this study, a new adsorbent material $NiFe_2O_4@SiO_2$–PEI which is polyethylene imine (PEI) grafted on core-shell $NiFe_2O_4@SiO_2$ nanoparticles was synthesized through a simple and easy procedure and characterized using PXRD, FE-SEM, EDX, FT-IR, and TGA-DTA analyses. The potential of $NiFe_2O_4@SiO_2$–PEI in the adsorption of CrO_4^{2-}, Ni^{2+}, and Pb^{2+} ions from aqueous solutions were investigated under variation of pH, adsorbent amount, metal ion concentration, and temperature. The maximum adsorption was achieved at pH = 6.5 and 250 mg/L CrO_4^{2-}, Ni^{2+}, and Pb^{2+} ions concentration and 0.075 g adsorbent at room temperature. The adsorption mechanism was investigated using pseudo-first order, pseudo-second order, and Elovich models with the best match of the pseudo-first order model with the experimental results. The best fit to the adsorption isotherms was the Langmuir model and both findings are in line with a smooth homogeneous mono-layer adsorption. The adsorption of both the anionic CrO_4^{2-}, and the cations Ni^{2+}, and Pb^{2+} ions increased with increasing time and decreased with increasing temperature and also the pH-dependency was very similar. Deconvolution of the *T*-dependent adsorption gave negative values for ΔG, ΔH and ΔS. For the metal cations Pb^{2+} and Ni^{2+} this is in line with binding of these cations to the amine-functions of the PEI. The very similar behavior of the anionic CrO_4^{2-} is probably due to reduction of CrO_4^{2-} to Cr^{3+} which shows comparable binding properties to Pb^{2+} and Ni^{2+}. In future studies we will elaborate on this using XPS for the determination of the oxidation states of the Cr species bound to the adsorbent.

For the moment we can state that the new adsorbent material $NiFe_2O_4@SiO_2$–PEI is an interesting candidate for removal of toxic metals from wastewater, in view of its simple preparation, simple

adsorbing kinetics, exothermic thermodynamics (chemical binding) and good recovery and recyclability. In the future we will further explore its potential by studying the adsorption of further metal cations such as Cu^{2+}, Cr^{3+}, and Gd^{3+} as well as the co-dependence of the adsorption of toxic metals with other cationic and anionic components in wastewater.

Author Contributions: The experimental work has been carried out by M.Kj., S.M.K., M.Z., and E.T.A. The original draft was written by M.Kj., A.K. and both authors have edited and revised the original draft. All authors agree with the submitted version of the manuscript.

Funding: E.T.A and A.K. acknowledge funding by the German Academic Exchange Service (DAAD; Eric Tobechukwu Anthony 91732061).

Availability of data and materials: Data will be made available on request.

Declarations Ethical approval: Not applicable

Acknowledgments: Laboratory support by the Islamic Azad University, Buinzahra Branch is highly acknowledged.

Competing interests: The authors declare that they have no known competing financial interests or personal relationships that could have appeared to influence the work reported in this paper.

TOC text:

Polyethyleneimine (PEI) was covalently bound to $NiFe_2O_4$@SiO_2 nanoparticles to form the new magnetically-separable material $NiFe_2O_4$@SiO_2–PEI for the adsorption of CrO_4^{2-}, Ni^{2+}, and Pb^{2+} ions from aqueous solutions.

References

1. Kaim, W.; Schwederski, B.; Klein, A. Bioinorganic Chemistry: Inorganic Elements in the Chemistry of Life, Wiley Chichester 2nd. ed. **2013**, ISBN: 978-1-118-65926-7.
2. Duffus, J.H. "Heavy Metals"—A Meaningless Term? (IUPAC Technical Report). *Pure Appl. Chem*. **2002**, *74*, 793–807. https://doi.org/10.1351/pac200274050793
3. Ethaib, S.; Al-Qutaifia, S.; Al-Ansari, N.; Zubaidi, S.L. Function of Nanomaterials in Removing Heavy Metals for Water and Wastewater Remediation: A Review. *Environments* **2022**, *9*, 123. https://doi.org/10.3390/environments9100123.
4. Damiri, F.; Andra, S.; Kommineni, N.; Balu, S.K.; Bulusu, R.; Boseila, A.A.; Akamo, D.O., Ahmad, Z.; Khan, F.S.; Rahman, Md.H.; Berrada, M.; Cavalu, S. Recent Advances in Adsorptive Nanocomposite Membranes for Heavy Metals Ion Removal from Contaminated Water: A Comprehensive Review. *Materials* **2022**, *15*, 5392. https://doi.org/10.3390/ma15155392
5. Liu, C.; Zhang, H.-X. Modified-biochar adsorbents (MBAs) for heavy-metal ions adsorption: A critical review. *J. Environ. Chem. Eng*. **2022**, *10*, 107393. https://doi.org/10.1016/j.jece.2022.107393
6. Mo, Z.; Tai, D.Z.; Zhang, H.; Shahab, A. A comprehensive review on the adsorption of heavy metals by zeolite imidazole framework (ZIF-8) based nanocomposite in water. *Chem. Eng. J.* **2022**, *443*, 136320. https://doi.org/10.1016/j.cej.2022.136320
7. Li, Y.; Yu, H.; Liu, L.; Yu, H. Application of co-pyrolysis biochar for the adsorption and immobilization of heavy metals in contaminated environmental substrates. *J. Hazard. Mater.* **2021**, *420*, 126655. https://doi.org/10.1016/j.jhazmat.2021.126655
8. Farouz, M.; El-Dek, S.I.; ElFaham, M.M.; Eldemerdash, U. Ecofriendly sustainable synthetized nano-composite for removal of heavy metals from aquatic environment. *Appl. Nanosci.* **2022**, *12*, 1585–1600. https://doi.org/10.1007/s13204-021-02331-3
9. Zhu, F.; Zheng, Y.-M.; Zhang, B.-G.; Dai, Y.-R. A critical review on the electrospun nanofibrous membranes for the adsorption of heavy metals in water treatment. *J. Hazard. Mater.* **2021**, *401*, 123608. https://doi.org/10.1016/j.jhazmat.2020.123608
10. Demirbas, A. Heavy metal adsorption onto agro-based waste materials: A review. *J. Hazard. Mater.* **2008**, *157*, 220–229. https://doi.org/10.1016/j.jhazmat.2008.01.024
11. Zhang, H.; Hu, X.; Li, T.; Zhang, Y.; Xu, H.; Sun, Y.; Gu, X.; Gu, C.; Luo, J.; Gao, B. MIL series of metal organic frameworks (MOFs) as novel adsorbents for heavy metals in water: A review. *J. Hazard. Mater.* **2022**, *429*, 128271. https://doi.org/10.1016/j.jhazmat.2022.128271
12. Soliman, N.K.; Moustafa, A.F. Industrial solid waste for heavy metals adsorption features and challenges; a review. *J. Mater. Res. Technol.* **2020**, *9*, 10235–10253. https://doi.org/10.1016/j.jmrt.2020.07.045
13. Talukder, M.E.; Pervez, M.N.; Jianming, W.; Stylios, G.K.; Hassan, M.M.; Song, H.; Naddeo, V.; Figoli, A. Ag nanoparticles immobilized sulfonated polyethersulfone/polyethersulfone electrospun nanofiber membrane for the removal of heavy metals. *Sci. Rep.* **2022**, *12*, 5814. https://doi.org/10.1038/s41598-022-09802-9

14. Wu, H.; Lin, G.; Liu, C.; Chu, S.; Mo, C.; Liu, X. Progress and challenges in molecularly imprinted polymers for adsorption of heavy metal ions from wastewater. *Trends Environ Anal Chem.* **2022**, *36*, e00178. https://doi.org/10.1016/j.teac.2022.e00178
15. Bao, S.; Yang, W.; Wang, Y.; Yu, Y.; Sun, Y.; Li, K. PEI grafted amino-functionalized graphene oxide nanosheets for ultrafast and high selectivity removal of Cr(VI) from aqueous solutions by adsorption combined with reduction: Behaviors and mechanisms. *Chem. Engin. J.* **2020**, *399*, 125762. https://doi.org/10.1016/j.cej.2020.125762
16. Godiya, C.B.; Liang, M.; Sayed, S.M.; Li, D.; Lu, X. Novel alginate/polyethyleneimine hydrogel adsorbent for cascaded removal and utilization of Cu^{2+} and Pb^{2+} ions. *J. Environ. Manag.* **2019**, *232*, 829–841. https://doi.org/10.1016/j.jenvman.2018.11.131
17. Jia, C.; Zhao, J.; Lei, L.; Kang, X.; Lu, R.; Chen, C.; Li, S.; Zhao, Y.; Yang, Q.; Chen, Z. Novel magnetically separable anhydride-functionalized Fe_3O_4@SiO_2@PEI-NTDA nanoparticles as effective adsorbents: synthesis, stability and recyclable adsorption performance for heavy metal ions. *RSC Adv.* **2019**, *9*, 9533–9545. https://doi.org/10.1039/C8RA10310K
18. Chen, S.; Wang, J.; Wu, Z.; Deng, Q.; Tu, W.; Dai, G.; Zeng, Z.; Deng, S. Enhanced Cr(VI) removal by polyethylenimine- and phosphorus-codoped hierarchical porous carbons. *J. Coll. Interfac. Sci.* **2018**, *523*, 110–120. https://doi.org/10.1016/j.jcis.2018.03.057
19. Jin, X.; Xiang, Z.; Liu, Q.; Chen, Y.; Lu, F. Polyethyleneimine-Bacterial Cellulose Bioadsorbent for Effective Removal of Copper and Lead Ions from Aqueous Solution. *Biores. Technol.* **2017**, *244*, 844–849. https://doi.org/10.1016/j.biortech.2017.08.072
20. Tomonaga, H.; Tanigaki, Y.; Hayashi, K.; Matsuyama, T.; Ida, J. Adsorption properties of poly(NIPAM-co-AA) immobilized on silica-coated magnetite nanoparticles prepared with different acrylic acid content for various heavy metal ions. *Chem. Eng. Res. Des.* **2021**, *171*, 213–224. https://doi.org/10.1016/j.cherd.2021.05.005
21. Zhang, L.; Guo, J.; Huang, X.; Wang, W.; Sun, P.; Li, Y.; Han, J. Functionalized biochar-supported magnetic $MnFe_2O_4$ nanocomposite for the removal of Pb(II) and Cd(II). *RSC Adv.* **2019**, *9*, 365–376. https://doi.org/10.1039/C8RA09061K
22. Wang, J.; Zheng, S.; Shao, Y.; Liu, J.; Xu, Z.; Zhu, D. Amino-functionalized Fe_3O_4@SiO_2 core-shell magnetic nanomaterial as a novel adsorbent for aqueous heavy metals removal. *J. Colloid Interface Sci.* **2010**, *349*, 293–299. https://doi.org/10.1016/j.jcis.2010.05.010
23. Xu, Y.; Li, Y.; Ding, Z. Network–Polymer–Modified Superparamagnetic Magnetic Silica Nanoparticles for the Adsorption and Regeneration of Heavy Metal Ions. *Molecules* **2023**, *28*, 7385. https://doi.org/10.3390/molecules28217385
24. Zeng, X.; Zhang, G.; Zhu, J.; Wu, Z. Adsorption of heavy metal ions in water by surface functionalized magnetic composites: a review. *Environmental Science: Water Res. Technol.* **2022**, *8*, 907–925. https://doi.org/10.1039/D1EW00868D
25. Thomas, B.; Alexander, L.K. Enhanced synergetic effect of Cr(VI) ion removal and anionic dye degradation with superparamagnetic cobalt ferrite meso–macroporous nanospheres. *Appl. Nanosci.* **2018**, *8*, 125–135. https://doi.org/10.1007/s13204-018-0655-6
26. Sureshkumar, V.; Daniel, S.C.G.K.; Ruckmani, K.; Sivakumar, M. Fabrication of chitosan–magnetite nanocomposite strip for chromium removal. *Appl. Nanosci.* **2016**, *6*, 277–285. https://doi.org/10.1007/s13204-015-0429-3
27. Shirsath, D.S.; Shirivastava, V.S. Adsorptive removal of heavy metals by magnetic nanoadsorbent: an equilibrium and thermodynamic study. *Appl. Nanosci.* **2015**, *5*, 927–935. https://doi.org/10.1007/s13204-014-0390-6
28. Zhang, J.; Ren, H.; Fan, H.; Zhou, S.; Huang, J. One-Step Fabrication of Recyclable Konjac Glucomannan-Based Magnetic Nanoparticles for Highly Efficient Cr(VI) Adsorption. *Molecules* **2023**, *28*, 7100. https://doi.org/10.3390/molecules28207100
29. Habila, M.A.; AlOthman, Z.A.; El-Toni, A.M.; Labis, J.P.; Khan, A.; Al-Marghany, A.; Elafifi, H.E. One-Step Carbon Coating and Polyacrylamide Functionalization of Fe_3O_4 Nanoparticles for Enhancing Magnetic Adsorptive-Remediation of Heavy Metals. *Molecules* **2017**, *22*, 2074; https://doi.org/10.3390/molecules22122074
30. Khalaj, M.; Taherkhani, M.; Kalhor, M. Preparation of some chromeno[4,3-d]pyrido[1,2-a]pyrimidine derivatives by ultrasonic irradiation using $NiFe_2O_4$@SiO_2 grafted di(3-propylsulfonic acid) nanoparticles. *New J. Chem.* **2021**, *45*, 10718–10724. https://doi.org/10.1039/D1NJ01676H
31. Xiang, B.; Ling, D.; Lou, H.; Gu, H. 3D hierarchical flower-like nickel ferrite/manganese dioxide toward lead(II) removal from aqueous water. *J. Hazard. Mater.* **2017**, *325*, 178–188. https://doi.org/10.1016/j.jhazmat.2016.11.011
32. Zhou, L.; Ji, L.; Ma, P.-C.; Shao, Y.; Zhang, H.; Gao, W.; Li, Y. Development of carbon nanotubes/$CoFe_2O_4$ magnetic hybrid material for removal of tetrabromobisphenol A and Pb(II). *J. Hazard. Mater.* **2014**, *265*, 104–114. http://dx.doi.org/10.1016/j.jhazmat.2013.11.058

33. Xu, W.; Song, Y.; Dai, K.; Sun, S.; Liu, G.; Yao, J. Novel ternary nanohybrids of tetraethylenepentamine and graphene oxide decorated with $MnFe_2O_4$ magnetic nanoparticles for the adsorption of Pb(II). *J. Hazard. Mater.* **2018**, *358*, 337–345. https://doi.org/10.1016/j.jhazmat.2018.06.071
34. Mahmoud, M.E.; Amira, M.F.; Seleim, S.M.; Mohamed, A.K. Amino-decorated magnetic metal-organic framework as a potential novel platform for selective removal of chromium(VI), cadmium(II) and lead(II). *J. Hazard. Mater.* **2020**, *381*, 120979. https://doi.org/10.1016/j.jhazmat.2019.120979
35. Huang, Y.; Zheng, H.; Hu, X.; Wu, Y.; Tang, X.: He, Q.; Peng, S. Enhanced selective adsorption of lead(II) from complex wastewater by DTPA functionalized chitosan-coated magnetic silica nanoparticles based on anion-synergism. *J. Hazard. Mater.* **2022**, *422*, 126856. https://doi.org/10.1016/j.jhazmat.2021.126856
36. Guo, X.; Du, B.; Wei, Q.; Yang, J.; Hu, L.; Yan, L.; Xu, W. Synthesis of amino functionalized magnetic graphenes composite material and its application to remove Cr(VI), Pb(II), Hg(II), Cd(II) and Ni(II) from contaminated water. *J. Hazard. Mater.* **2014**, *278*, 211–220. https://doi.org/10.1016/j.jhazmat.2014.05.075
37. Huang, Y.; Wang, B.; Lv, J.; He, Y.; Zhang, H.; Li, W.; Li, Y.; Wågberg, T.; Hu, G. Facile synthesis of sodium lignosulfonate/polyethyleneimine/sodium alginate beads with ultra-high adsorption capacity for Cr(VI) removal from water. *J. Hazard. Mater.* **2022**, *436*, 129270. https://doi.org/10.1016/j.jhazmat.2022.129270
38. Yanovska, E.; Savchenko, I.; Petrenko, O.; Davydov, V. Adsorption of some toxic metal ions on pine sawdust in situ immobilized by polyaniline. *Appl. Nanosci.* **2022**, *12*, 861–868. https://doi.org/10.1007/s13204-021-01862-z
39. Siddiqui, S.H. The removal of Cu^{2+}, Ni^{2+} and Methylene Blue (MB) from aqueous solution using Luffa Actangula Carbon: Kinetics, thermodynamic and isotherm and response methodology. *Groundwater Sust. Develop.* **2018**, *6*, 141–149. https://doi.org/10.1016/j.gsd.2017.12.008
40. Zhao, Y.-G.; Shen, H.-Y.; Pan, S.-D.; Hu, M.-Q. Synthesis, characterization and properties of ethylenediamine-functionalized Fe_3O_4 magnetic polymers for removal of Cr(VI) in wastewater. *J. Hazard. Mater.* **2010**, *182*, 295–302. https://doi.org/10.1016/j.jhazmat.2010.06.029
41. Guo, D.-M.; An, Q.-D.; Xiao, Z.-Y.; Zhai, S.-R.; Yang, D.-J. Efficient removal of Pb(II), Cr(VI) and organic dyes by polydopamine modified chitosan aerogels. *Carbohydr. Polym.* **2018**, *202*, 306–314. https://doi.org/10.1016/j.carbpol.2018.08.140
42. Wang, X.; Li, X.; Peng, L.; Han, S.; Hao, C.; Jiang, C.; Wang, H.; Fan, X. Effective removal of heavy metals from water using porous lignin-based adsorbents. *Chemosphere* **2021**, *279*, 130504. https://doi.org/10.1016/j.chemosphere.2021.130504
43. Wang, X.; Xu, J.; Liu, J.; Liu, J.; Xia, F.; Wang, C.; Dahlgren, R.A.; Liu, W. Mechanism of Cr(VI) removal by magnetic greigite/biochar composites. *Sci. Total Environ.* **2020**, *700*, 134414 https://doi.org/10.1016/j.scitotenv.2019.134414
44. Wang, Y.; Yang, Q.; Chen, J.; Yang, J.; Zhang, Y.; Chen, Y.; Li, X.; Du, W.; Liang, A.; Ho, S.-H.; Chang, J.-S. Adsorption behavior of Cr(VI) by magnetically modified Enteromorpha prolifera based biochar and the toxicity analysis. *J. Hazard. Mater.* **2020**, *395*, 122658 https://doi.org/10.1016/j.jhazmat.2020.122658
45. Cai, W.; Dionysiou, D.D.; Fu, F.; Tang, B. CTAB–intercalated molybdenum disulfide nanosheets for enhanced simultaneous removal of Cr(VI) and Ni(II) from aqueous solutions. *J. Hazard. Mater.* **2020**, *396*, 122728. https://doi.org/10.1016/j.jhazmat.2020.122728
46. Huang, Y.; Lee, X.; Macazo, F.C.; Grattieri, M.; Cai, R.; Minteer, S.D. Fast and Efficient Removal of Chromium(VI) Anionic Species by a Reusable Chitosan-Modified Multi-Walled Carbon Nanotube Composite. *Chem. Engin. J.* **2018**, *339*, 259–267. https://doi.org/10.1016/j.cej.2018.01.133
47. Largitte, L.; Pasquier, R. A review of the kinetics adsorption models and their application to the adsorption of lead by an activated carbon. *Chem. Eng. Res. Des.* **2016**, *109*, 495–504. http://dx.doi.org/10.1016/j.cherd.2016.02.006
48. Ghashang, M.; Khosravian, P.; Ghayoor, H. Effective removal of penicillin from aqueous solution using Zinc oxide/natural-Zeolite composite nano-powders prepared via ball milling technique. *Rec. Pat. Nanotechnol.* **2017**, *11*, 154–164. https://doi.org/10.2174/1872210511666170105141550
49. Langmuir, I. The constitution and fundamental properties of solids and liquids. Part I. Solids. *J. Am. Chem. Soc.* **1916**, *38*, 2221–2295. https://doi.org/10.1021/ja02268a002
50. Freundlich, H. On adsorptions in solution. *Z. Phys. Chem.* **1907**, *57*, 385–471. https://doi.org/10.1515/zpch-1907-5723
51. Haghighatian, S.; Mazarei, E.; Doroodmand, M.M.; Klein, A., Memarpoor-Yazdi, M. A new whole-cell biocatalyst for sulfur dioxide filtering and degradation. *Biores. Technol.* **2020**, *314*, 123755. https://doi.org/10.1016/j.biortech.2020.123755